Macroscopic Modeling of *In Vivo* Drug Transport in Electroporated Tissue

Bradley Boyd[a] and Sid Becker[a]

[a]Department of Mechanical Engineering, University of Canterbury, Christchurch, New Zealand

(E-mail: bradley.boyd@pg.canterbury.ac.nz).

(E-mail: sid.becker@canterbury.ac.nz)

NOMENCLATURE

SYMBOLS

A	Area [m^2]
C	Intrinsic volume averaged concentration [kg/m^3]
C^*	Dimensionless concentration
C_e	Intrinsic volume averaged extracellular concentration [kg/m^3]
C_i	Intrinsic volume averaged intracellular concentration [kg/m^3]
D	Diffusivity [m^2/s]
DOE	Degree of electroporation
DOE_R	Transient degree of electroporation
E	Electric field magnitude [V/m]
IE	Fraction of irreversible electroporation
L^2	L^2 normalized error
NOP	Number of solution nodes
m^*	Dimensionless mass delivered to viable cells
t	Time [s]
t_p	Time elapsed since the end of the previous electroporation pulse [s]
X	Solution of interest
x, y, z	Cartesian space coordinates [m]
v	Volume [m^3]

GREEK LETTERS

ε	Porosity
θ	Maximum relative difference between solutions
μ_R	Mass transfer coefficient of the cell membrane [1/s]
τ	Cellular permeability decay constant [s]
ϕ	Electrical potential [V]
ω	Numerical damping factor

SUBSCRIPTS

eff	Effective
e	Extracellular space
i	Intracellular space

SUPERSCRIPTS

p	Current iteration
$p-1$	Previous iteration

ABSTRACT

This study develops a macroscopic model of mass transport in electroporated biological tissue in order to predict the cellular drug uptake. The changes in the macroscopic mass transport coefficient of cellular drug uptake are related to the empirically determined increases in electrical conductivity. Additionally, the model considers the influences of both irreversible electroporation and the transient resealing of the cell membrane associated with reversible electroporation. Two case studies are conducted to illustrate the applicability of this model by comparing transport associated with two electrode arrangements: side-by-side arrangement and the clamp arrangement. The results show increased drug transmission to viable cells is possible using the clamp arrangement due to the more uniform electric field.

Keywords: Electroporation, Electropermeabilization, Diffusion, Mass Transport, Mathematical Modeling.

1. INTRODUCTION

The basic structure of the cell membrane, the bilayer lipid membrane (BLM), consists of two layers of phospholipid molecules typically 5 nm thick [1]. The cell membrane separates the intracellular space (containing cytoplasm) from the extracellular space and its function is to protect the cytoplasm by regulating the molecular transfer. This barrier function must be overcome for the successful cellular uptake of a drug. Electroporation is one method that is used to overcome the cell's barrier function by disrupting the structure of the membrane.

The empirically based explanation of the electroporation of the cell membrane follows the transient aqueous pore mechanism hypothesis [2-4]. The transient aqueous pore mechanism involves a sudden localized transition to water filled pores in the membrane structure during the application of a short duration (1 μs to 100 ms) – high voltage electric pulse [5]. Recovery of the membrane (the transition of hydrophilic pores back to the BLM structure) is known to occur unless the membrane is irreversibly electroporated [2-4]. In some cases, the reversible electropores can be "long lived" lasting several minutes to hours [6, 7]. These long lasting, reversible electropores can provide the sustained permeability increases that are required to facilitate the relatively slow diffusion process of the transport of a drug into the cytoplasm.

The introduction of the electropores is described to occur in a sequential process: the charging of the cell membrane, the creation of the pores, and the evolution of the pores. An excellent numerical and theoretical representation of the development of the electropores in single cell electroporation is provided in Ref [2]. The formation of these defects in bilayer membranes has also been predicted in simulations at the molecular scale [8-10]. The timescale associated with the initiation and evolution of the electropores depends on the magnitude of the electrical field, but is considered to occur at or below

the order of μs [2]. Our knowledge of electroporation at the cellular level allows for the prediction (on an individual cell) of the number of pores, the pore sizes, and the fraction of the cell membrane that is occupied by these pores [2, 11].

The challenge for researchers is to apply the understanding of this short timescale single cell behavior to the much slower phenomena associated with macroscale transport. In order to represent the effects of electroporation on macroscopic transport, the following important points that should be addressed: the increases in cellular permeability, the pore resealing, any cell death associated with the electric field, and the changes in the bulk tissue electrical conductivity during the electric pulse.

The term irreversible electroporation refers to the situation in which the pores created by electroporation are unable to reseal over time [12, 13]. This non-thermal irreversible electroporation is reported to occur when the electric field experienced by a cell membrane exceeds a threshold value [12, 13]. The result of irreversible electroporation is a compromised functionality of the cell, which leads to cell death. While the specific mechanism for cell death is still unclear [14], it is generally accepted that the process of cell death is necrosis due the pores not resealing. A model that attempts to predict the cellular uptake of drug should also account for irreversible electroporation in regions of tissue exposed to extreme electric fields.

When the transmembrane voltage is below the threshold for irreversible electroporation, the electropermeabilization of the cell membrane is not permanent. The complete membrane recovery associated with reversible electroporation has been shown to occur on a timescale of seconds to minutes [3] and the rate has been determined experimentally [15]. Because this process of pore resealing can occur on a similar timescale as macroscopic diffusion, mass transport models that are dominated by the process of diffusion should consider the effects of pore-resealing.

One of the most drastic macroscale effects of electroporation concerns the increases in electrical conductivity of the bulk tissue [16]. The increase in electrical conductivity at the tissue level is due to the formation of aqueous electropores in the cell membrane. In fact, the change in the bulk tissue electrical conductivity is considered a good indicator of the increases in permeability resulting from electroporation [11, 12, 16-20]. The electroporation in biological tissue has previously been modeled numerically by relating the changes in the electrical conductivity to the magnitude of the electric field [16, 21-23].

Addressing the modeling of drug delivery following electroporation from a macroscopic perspective is a relatively recent development. The 2003 study by Puc et al. [11] develops a combined theoretical-experimental based two-compartment pharmakinetic model that relates the magnitude of cell electroporation to the electric field and incorporates the effects of pore resealing and cell death by irreversible electroporation. However, that study does not capture the macroscopic spatial variations in drug concentration and cellular permeability.

The first attempt to capture the large scale spatial responses of the delivery of drugs in electroporated tissue was conducted by Granot and Rubinsky in their 2008 work [24]. In that study, the authors adapt the model of single cell electroporation by Krassowska [2] so that it can be used to describe the state of the electropores as a function of the local electrical field and allows for the effects of resealing to be considered. This in turn is related to the ability to transport the drug from the extracellular to the intracellular space. The model does not consider that the electrical conductivity of the tissue is also related to the cellular permeability during electroporation, nor does it include the effects of cell death by irreversible electroporation.

The most recent progression is the 2014 work of the Miklavčič group in Ref. [25]. This study captures the spatially dependent diffusion of the drug in the tissue and is the first study to thoroughly connect the electroporation induced permeability increases to the macroscopic transport and cellular uptake of the drug. This paper develops a description of the mass transport coefficient, which represents the permeability increases of the cell membrane that are associated with the electropores. However, that study assumes a uniform electric field, and the model does not include the effects of irreversible electroporation.

In the present study, we extend the previous models [11, 24, 25] that relate the effects of electroporation to the delivery of drugs in biological tissue. We use existing empirically based relationships to predict the tissue electrical conductivity based on the electric field. We then use these changes in the electrical conductivity to quantify the increases in cellular permeability to the drug. The changes in electrical conductivity are also used to quantify the extent of cell death by irreversible electroporation. This study also considers pore resealing after the electroporation. This model is then applied to two-dimensional transient case studies in order to showcase the model's ability to capture the "large scale" spatial variations in the electric field and the subsequent cellular uptake of the drug.

2. THEORETICALLY MODELING ELECTROPORATION

This section provides the description of a theoretical representation of electroporation and relates this to the transport of the drug into electroporated cells. The theoretical components presented in the following section are considered from a macroscopic perspective. Some of these have been previously developed. The distinction of this work is that the electric field dependent increases in electrical conductivity are used to represent the extent of permeability increases that subsequently can be used to predict the rate of drug exchange from the extracellular to the intracellular space.

2.1. ELECTROPORATION

Previous experimental and theoretical studies have shown that the extent to which cells are electroporated is dependent on the magnitude of the electric field resulting from the applied electroporation pulse [2-5, 8-16, 18-24, 26-45]. Thus, the discussion begins with the modeling of the electric field. In general, the Laplace equation is used to describe the distribution of the electrical potential:

$$\nabla \cdot (\sigma \cdot \nabla \phi) = 0 \tag{1}$$

where σ is the electrical conductivity and ϕ is the electrical potential. This representation has been supported experimentally [12, 16, 20, 23] and has been used to model the electric field associated with electroporation in numerous theoretical studies [12, 13, 16, 20-23, 34, 40, 44, 45]. Theoretically, Eq. (1) assumes the current density is divergence free: this assumption can be made if any non-Ohmic behavior is negligible [22, 23]. In macroscopic experimental studies, the measurable effects associated with electroporation (increases in electrical conductivity and permeability to ionic and molecular transport) are directly linked to the magnitude of electric field [12, 16, 19, 44]. The magnitude of electric field is simply the magnitude of the gradient in the electric potential:

$$E = |\nabla \phi| \tag{2}$$

Note that the electrical conductivity of Eq. (1) is expected to increase as the cells (composing the tissue) are electroporated. The prediction of this change in electrical conductivity is discussed next.

2.1.1. ELECTRICAL CONDUCTIVITY CHANGES

At the cellular level, electroporation results in the creation of individual pores in the cell membrane. From a macroscopic perspective, these pores have the effect of increasing the electrical conductivity (measured as increases in electrical current) of the bulk tissue that is composed of these electroporated cells [16-18]. As the electric field increases above the onset threshold for reversible electroporation, more cells are electroporated. This results in a smooth saturation of electroporated cells in the tissue

[16]. Previous studies have considered various functional dependencies of the electrical conductivity on the electric field magnitude (E) [12, 16, 20, 22, 23]. A combined experimental and computational study [12] develops an empirically based sigmoidal dependency of effective electrical conductivity on the magnitude of the electric field that is depicted in Fig. 1 and represented as:

$$\sigma(E) = \frac{\sigma_{\max} - \sigma_{\min}}{1 + \alpha \cdot \exp\left[-\frac{E-a}{b}\right]} + \sigma_{\min} \qquad (3)$$

$$a = \frac{E_{rev} + E_{irrev}}{2} \qquad b = \frac{E_{irrev} - E_{rev}}{\beta}$$

In this approximation, the term E_{rev} represents the onset threshold electric field magnitude for reversible electroporation. This is the minimum electric field magnitude required for any reversible electroporation to occur. Below this value, the electric field is not sufficient to initiate any electroporation. The term E_{irrev} refers to the onset threshold electric field magnitude required for irreversible electroporation (or the onset of a loss in cell viability). The value of E_{irrev} can be found experimentally by determining the onset at which cell necrosis is observed. For example in section 2.4 of the paper by Miklavčič et al. [46] an explicit description of evaluating the threshold of the electric field magnitude at which rabbit liver cells begin to experience necrosis. Below this value, there is no irreversible electroporation of the cells. The value of the effective tissue electrical conductivity in the absence of any electroporation is denoted $\sigma_{\min}$. The maximum possible effective electrical conductivity of the tissue resulting from electroporation is denoted $\sigma_{\max}$. The symbols α and β are the sigmoidal functional parameters. The parameter values of Eq. (3) are dependent on the tissue and can be determined experimentally [16, 20, 44].

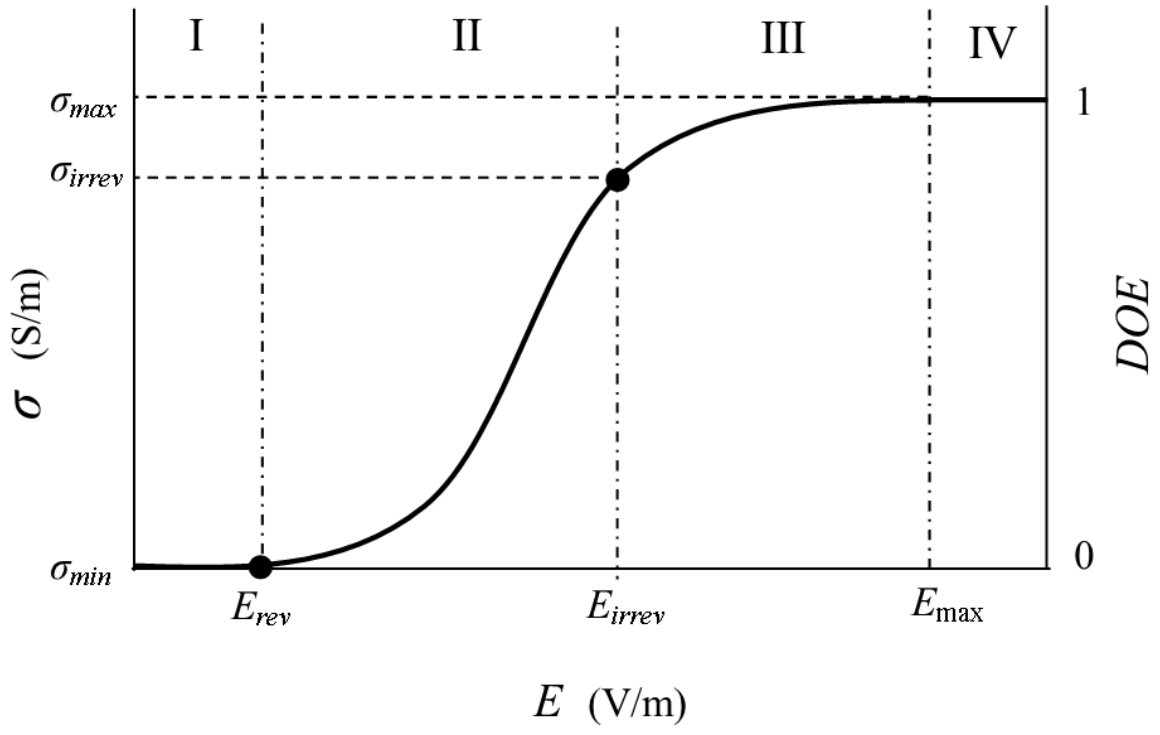

Fig. 1. The dependence of the electrical conductivity (**Error! Bookmark not defined.**) on the magnitude of the electric field (E) represented by Eq. (3) and simultaneously the degree of electroporation (DOE) represented by Eq. (4).

The state of tissue electroporation can be characterized by four key stages: (I) no electroporation, (II) reversible electroporation, (III) irreversible electroporation, and (IV) complete irreversible electroporation. These stages of tissue electroporation may be related to the electrical conductivity shown in Fig. 1. Stage I refers to no measurable increase in electrical conductivity and thus no electroporation. Stage II is where the distribution of cells composing the tissue are being electroporated to a reversible extent, significantly increasing the electrical conductivity. The extent of reversible electroporation increases smoothly due to the distribution of cell size resulting in a varying transmembrane voltage [47]. Stage III is past E_{irrev} (onset of loss of cell viability) resulting in a fraction of irreversibly electroporated cells [16]. In this stage of irreversible electroporation, the electrical conductivity begins to plateau as the electric field is increased, due to the electroporation approaching the limit. The limit refers to the magnitude of electric field where the entire population of cell subjected are irreversibly electroporated ($E_{\max}$) - stage IV. Beyond $E_{\max}$ no further alteration in the electrical conductivity takes place.

2.1.2. Degree of Electroporation

In order to relate the effects of electroporation to the increases in cellular permeability, it is first necessary to quantify the extent to which the cells are electroporated. It is generally accepted that the

increases in the electrical conductivity are directly representative of the extent to which cells in the tissue have been electroporated [16-18]. This is because the increases in measured electrical conductivity are a consequence of the introduction of aqueous pores in the cell membrane. We next relate the extent of cellular electroporation to the increases in the electrical conductivity by a function we will call the degree of electroporation (DOE), which is defined by the relation:

$$DOE(E) = \frac{\sigma(E) - \sigma_{\min}}{\sigma_{\max} - \sigma_{\min}} \tag{4}$$

In this way, the DOE (also depicted in Fig. 1) follows the same smooth dependency on the magnitude of the electric field as the effective electrical conductivity. A zero value of the DOE indicates that no electroporation has occurred, and a DOE with the value unity indicates that no further electroporation can occur. From the macroscopic perspective and in the context of this study, the degree of electroporation can be interpreted as the link between the electric field and the increases of the cells' permeability to mass transport. This idea is revisited in the development of the mass transport model.

2.1.3. IRREVERSIBLE ELECTROPORATION

When the electric field magnitude is sufficiently high, the electroporation pores in the cell membrane are permanent and do not reseal over time. Irreversible electroporation causes cell death because it compromises the functionality of the cell [13, 14, 36, 37, 40, 41, 45]. It is necessary to quantify the extent of irreversible electroporation as it influences the membrane pore resealing and represents the extent of cell death. In the theoretical study Ref. [11] a function named the "survival fraction" is introduced to represent the effects of irreversible electroporation, following a sigmoidal dependence on the magnitude of electric field. Similarly, in this, study we consider once more the idea that the changes in the macroscopic electrical conductivity can be considered to directly represent the averaged state of the electropores in the cell membranes. Note that in stage III of Fig. 1, as the electric field magnitude (E) exceeds the onset of irreversible electroporation (E_{irrev}), the electrical conductivity asymptotically approaches its maximum value ($\sigma_{\max}$). The physical interpretation of the limiting-off effect is that as more of the electropores have reached their irreversible state (limit of electroporation) the electrical conductivities sensitivity to the change in electric field reduces. Since this process is so well reflected by the electrical conductivity, in this paper the extent of irreversible electroporation is quantified by the state of the electrical conductivity. Introducing a term called the fraction of irreversible electroporation (IE) represented by:

$$IE(E) = \begin{cases} 0 & \text{for } E < E_{irrev} \\ \dfrac{\sigma(E) - \sigma_{irrev}}{\sigma_{\max} - \sigma_{irrev}} & \text{for } E \geq E_{irrev} \end{cases} \tag{5}$$

where σ_{irrev} is the value of the electrical conductivity corresponding to the magnitude of the electric field at the onset threshold for irreversible electroporation (E_{irrev}) and the electrical conductivity in the numerator is evaluated from Eq. (3). This function is depicted in Fig. 2. An IE value of unity represents completely irreversibly electroporated tissue and a value of zero indicates that the electric field is below the threshold E_{irrev} and that none of the cells are damaged.

Considering that E_{irrev} corresponds to the onset of cell death ($IE = 0$) and $E_{\max}$ corresponds to the magnitude of electric field where the entire population of cells subjected are irreversibly electroporated ($IE = 1$); Eq. (5) provides a first order approximation of the fraction of irreversible electroporation (IE) using the changes in electrical conductivity between these two parameters (E_{irrev} and $E_{\max}$). This approximation (Eq. (5)) should be experimentally validated, but for the purposes of this representative study it provides valuable insights. Ideally, the fraction of irreversible electroporation (IE) could be redefined by empirically relating it directly to the magnitude of electric field, like the "survival fraction" developed in Ref. [11].

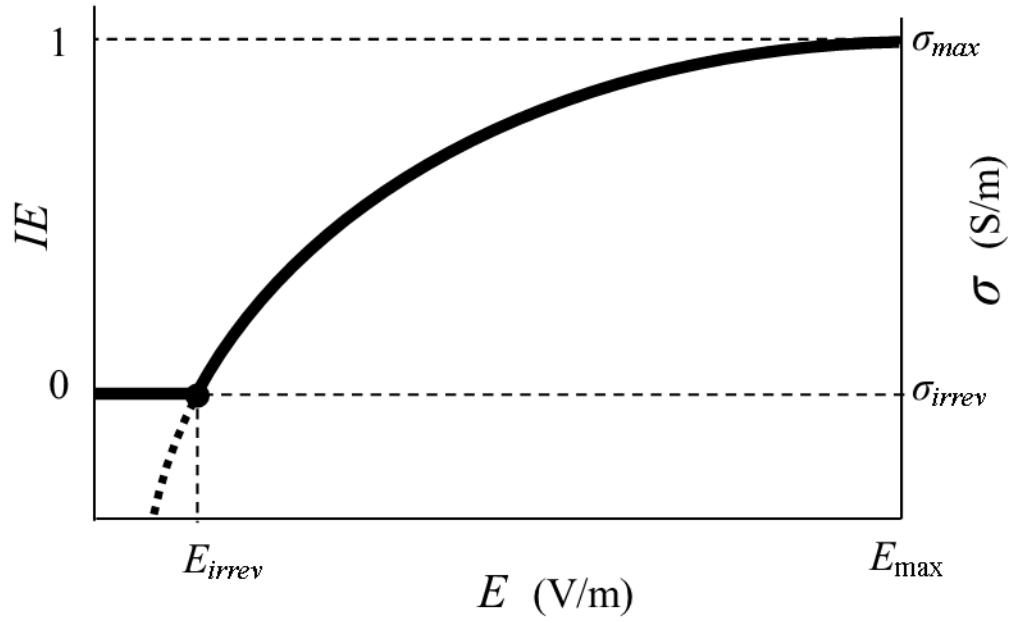

Fig. 2. The dependence of the fraction of irreversible electroporation (IE) (thick line) on the magnitude of electric field (E). The fraction of irreversible electroporation is approximated by Eq. (5) using the electrical conductivity (Eq. (3)) at values above the electrical conductivity associated with the onset of irreversible electroporation (σ_{irrev}).

2.1.4. PORE RESEALING: THE TRANSIENT DEGREE OF ELECTROPORATION

When cells are reversibly electroporated, they return to their original state over time [15]. Pore resealing is observed experimentally as a relaxation in the increases in the cell permeability associated with electroporation. The effects of reversible electroporation have been shown to diminish exponentially in time [30, 47-49]. In order to account for the transient resealing of the reversibly electroporated cells as well as the permanently irreversibly electroporated cells, the transient degree of electroporation is defined by the relation:

$$DOE_R(E,t) = DOE(E) \cdot \left(\left(1 - IE(E)\right) \cdot \exp\left[-\frac{t_p}{\tau} \right] + IE(E) \right) \tag{6}$$

where t_p is the time after the end of the previous electroporation pulse, and τ is the time constant for cell permeability relaxation (due to pore resealing) which may be determined experimentally. The DOE is evaluated from Eq. (4) and the IE is evaluated from Eq. (5). It should be noted that the magnitude of IE at a specific location can never decrease.

In the case of multiple electroporation pulses, the state of the electrical conductivity due to a previous electroporation pulse may also need to be considered. As the cells reseal, the electrical conductivity will also return to its original value. This can be addressed by relating the electrical conductivity to the transient degree of electroporation (DOE_R):

$$\sigma_R = DOE_R \cdot \left(\sigma_{\max} - \sigma_{\min} \right) + \sigma_{\min} \tag{7}$$

where σ_R is the electrical conductivity of the tissue. The implementation of the electrical conductivity into the electric potential distribution solver is discussed later.

The transient response of the bulk tissue conductivity is captured in Eq. (7) through the reversible degree of electroporation (DOE_R). The resealing of the electropores is addressed in Eq. (6) using an empirically determined time constant, so that the transient effect should be well represented in Eq. (7). The expression also considers that the irreversibly electroporated cells have no contribution to the transient electrical characteristics of the tissue. However, it should be noted that while the nature of this recovery is experimentally based, the magnitudes reflected by Eq. (7) have not been experimentally validated.

The motivation behind the attempt to quantify the magnitude of the electroporation and capture the effects of the pore resealing of Eq. (6) is ultimately to attempt to couple the effects of electroporation to the cellular uptake of the drug and to the general drug transport. The following sections describe the mass transport model and couple this to the transient degree of electroporation, DOE_R.

2.2. MASS TRANSPORT IN ELECTROPORATED TISSUE

In this section we will relate the transient degree of electroporation (DOE_R) to the mass transport. We first consider that from a macroscopic perspective the tissue may be considered to be a composition of two distinct regions:

1) The extracellular space that composes the space outside the cells. This extracellular space is a continuous space containing the extracellular matrix structure, which provides the support structure for the surrounding cells. The interstitial fluid occupies the rest of the extracellular space [50].
2) The intracellular space that represents the sum of all the discreet volumes that are encompassed by the individual cell walls. The intracellular space is the target of cellular drug delivery.

The two spaces, the extracellular and the intracellular, are separated by the cell membrane (Fig. 3). The cell membrane restricts the mass transfer from extracellular to intracellular space: the cellular drug uptake. Note that the drug is free to travel by diffusion throughout the extracellular space as it is continuous, however, once it arrives in the intracellular space, the drug is restricted from freely diffusing through the domain by the cell wall. The drug concentration in the extracellular space is denoted C_e and the drug concentration in the intracellular space is denoted C_i . These concentrations are macroscopic properties which are determined using the intrinsic volume averaged concentration [51]. This description is a porous media representation of the tissue where the fluid filled extracellular space is set within a solid matrix of cells. The relative measure of the extracellular space is represented by the porosity [51]:

$$\varepsilon = \frac{\mathrm{v}_e}{\mathrm{v}_e + \mathrm{v}_i} \tag{8}$$

Figure 3 shows the volumes of interest, where v_e is the extracellular space volume and v_i is the intracellular space volume.

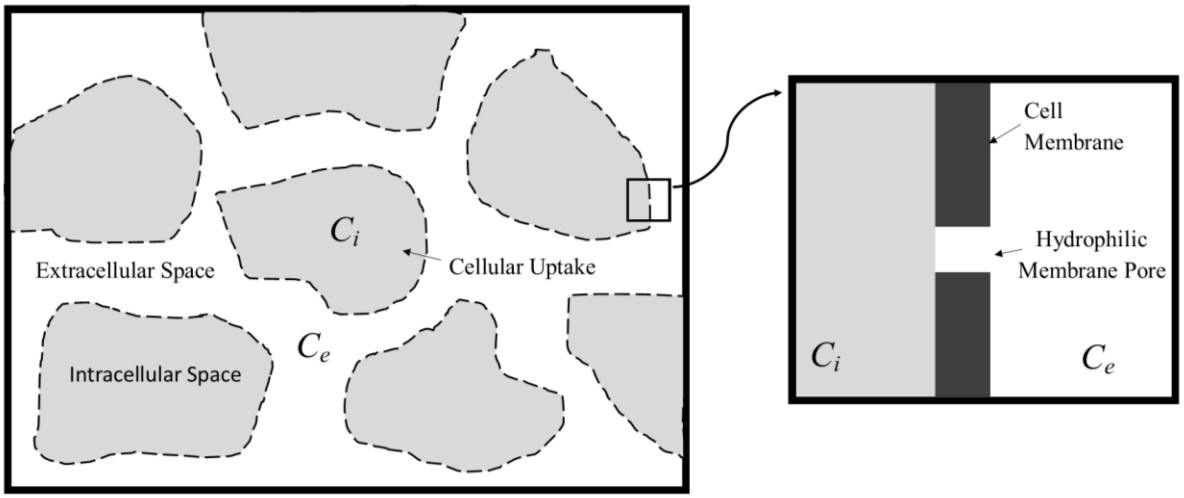

Fig. 3. A representation of the extracellular and intracellular space, cell membrane, and membrane pores.

The coupled extra-intracellular transport model used in this study follows the one developed by the research group of Miklavčič in ref. [43]. The concentration of the drug in the extracellular space (C_e) is governed by:

$$\frac{\partial C_e}{\partial t} = \nabla \cdot (D_{eff} \nabla C_e) - \frac{1-\varepsilon}{\varepsilon} \mu_R \cdot (C_e - C_i) \tag{9}$$

where D_{eff} is the effective diffusion coefficient of the drug in the extracellular space, which is either determined experimentally or approximated using the extracellular space tortuosity of the tissue [43, 51, 52]. The mass transfer coefficient, μ_R, is associated with the condition of the cell membrane, and governs the rate of cellular drug uptake. The last term of Eq. (9) represents the rate at which the drug leaves the extracellular space due to the cellular drug uptake. This is a diffusive process that occurs through the pores within the cell membrane, which separates the extracellular space from the intracellular space (see Fig. 3).

The drug concentration within the intracellular space is governed by:

$$\frac{\partial C_i}{\partial t} = \mu_R \cdot (C_e - C_i) \tag{10}$$

Note that Eqs. (9) and (10) do not consider the effects of partitioning, absorption, metabolism, or clearance [51]. Electrophoresis and electro-osmosis during the application of the electric pulse are also not considered in the development of this model.

The mass transport coefficient, μ_R, of Eqs. (9) has previously been formally defined by the Miklavčič's research group in Ref. [43]. In that study it is logically posed that the permeability of the cell membrane

to the solute (the magnitude of the mass transport coefficient) is directly proportional to the total area of all pores in the cell membrane. This is a very helpful contribution because the electroporation related increases in the total pore area can now be directly related to increases in the mass transport coefficient. It is the purpose of the current study to extend this idea in order to directly relate the drug uptake to the electroporation induced electric field. Recall that the transient degree of electroporation defined in Eq. (6) was developed in order to reflect the state of the cellular permeability after electroporation. With this in mind, we consider a simple linear dependence of the mass transport coefficient on the transient degree of electroporation (DOE_R):

$$\mu_R = DOE_R \cdot (\mu_{\max} - \mu_0) + \mu_0 \tag{11}$$

where $\mu_{\max}$ corresponds to the magnitude of the mass transfer coefficient when the cell is fully electroporated ($DOE_R = 1$). The parameter μ_0 represents the mass transfer in the case that the cells have experienced no electroporation ($DOE_R = 0$); it is probably negligible for larger solutes. The cellular uptake mass transfer coefficients ($\mu_{\max}$ and μ_0) are highly dependent on the solute, the cell type, and the electroporation parameters. Experimental measurements could be used in order to determine these values for a given solute, tissue, and pulse characteristic. A theoretical approximation of the parameters, $\mu_{\max}$ and μ_0 , is used based on the theoretical development of the mass transfer coefficient in Ref. [43].

It is important to note that the accuracy of Eq. (11) in predicting the behavior of the cells' permeability to molecular transport depends on how well the empirically derived transient degree of electroporation (DOE_R which is based on the bulk electrical behavior of the tissue) represents the state of the cell membrane. Expression (11) assumes that the rate of cellular recovery associated with the permeability of mass transport across the cell membrane is the same as that of the long term electrical recovery of the cell membrane. While in principle the mechanics are the same (both are associated with the resealing of the electropores), the validity of this expression has yet to be explicitly validated.

3. NUMERICAL MODEL

A numerical model is developed to illustrate the applicability of the theoretical model described in Section 2. The numerical model considers the evaluation of Eqs. (1)−(11) in a two dimensional domain. Two test cases are considered that are representative of two different electrode arrangements. In this section we discuss the numerical handling of the model.

3.1. GENERAL COMPUTATIONAL CONSIDERATIONS

The solutions of the governing Eqs. (1), (9), and (10) are approximated numerically using the finite volume approach. The transient equations governing the concentrations, Eqs. (9) and (10), are represented using a fully implicit scheme. The resulting discretized systems of equations are solved using the successive over-relaxation (SOR) method [53] where the convergence is determined from the relative maximum localized difference in solution between iterations (θ):

$$\theta = \max_{i=1,NOP}\left(\frac{\left\|X^{p}(i)-X^{p-1}(i)\right\|}{\max\limits_{i=1,NOP}\left\|X^{p-1}(i)\right\|}\right) \tag{12}$$

where $X^{p}(i)$ is the solution from the current iteration of the conserved variable $(\phi,\ C_i,$ or $C_e)$ and $X^{p-1}(i)$ corresponds to that of the previous iteration. The integer i corresponds to the node number and NOP is the number of nodes. Convergence is reached when $\theta \le 10^{-10}$.

A grid is used with increased refinement in regions of the domain where electroporation occurs, allowing the solution to be determined significantly faster without compromising the accuracy. To ensure the independence of the solution from the grid and time step used, grid and time-step independence studies were conducted. An L^2 normalized error, symbolized by L^2, was used to estimate the difference between the solutions of different resolutions:

$$L^2 = \sqrt{\frac{\sum_{i=1}^{NOP}\left(X^{p}(i)-X^{p-1}(i)\right)^2}{\sum_{i=1}^{NOP}\left(X^{p-1}(i)\right)^2}} \tag{13}$$

The resolution of the rectilinear grid was refined until an L^2 error norm (L^2) value of less than 0.001 was reached. This resulted in the number of spatial grid nodes provided in Table 2 for the cases modeled. Two time step sizes were considered: a larger time step size was used for the mass transport prior to the electroporation and a smaller time step size was considered after the initial electroporation pulse. The time step sizes were halved until an error (L^2) value of less than 0.001 was reached, resulting in the time step sizes provided in Table 2.

In order to verify the numerical handling of the conservation Eqs. (1) and (9), a comparison study is conducted of the numerical solution to a known analytical (exact) solution. A simple test case of a square region is depicted in Fig. 4: this has been amended from the problem presented in section 3.2.1 of the book Ref. [54]. The numerical solutions were evaluated for a square region with 40804 nodes. The numerical handling of the steady potential distribution is solved with a constant electrical conductivity, one inhomogeneous boundary, one homogenous boundary condition, and two insulated boundaries, as outlined in Fig. 4a. The numerical solution is then compared to the exact solution that is provided in Table 3.26 of reference [54]. The resulting error (L^2) is less than 0.0012.

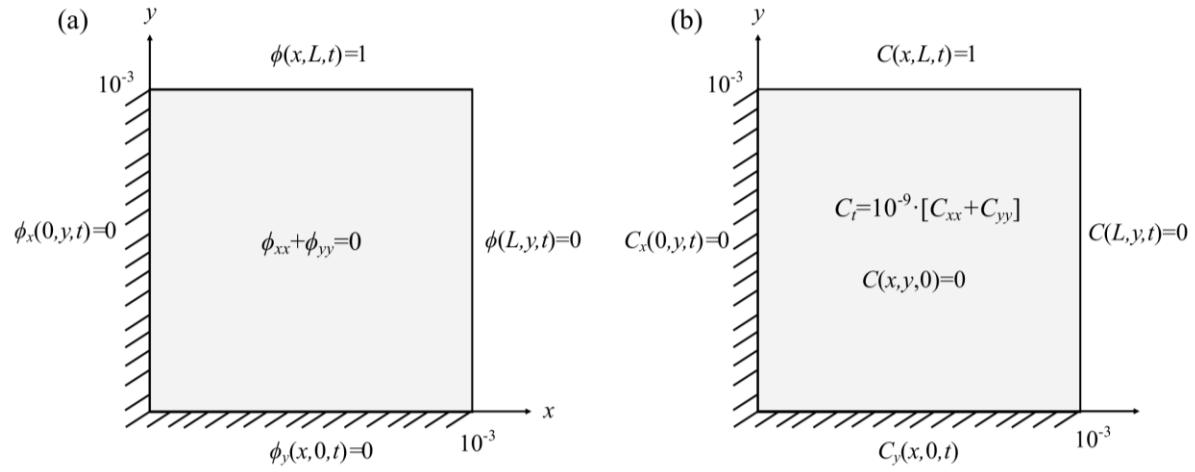

Fig. 4. The simplified case for verification of the numerical solver using the analytical solution. Where (a) is for the steady state electric potential (ϕ) distribution and (b) is for the transient concentration (C) distribution (where $\mu_R = 0$). The analytical solutions to these problems are provided in Ref. [54]

To verify (in part) the numerical handling of the extracellular concentration of Eq. (9) the simple transient case represented by Fig. 4b is considered. This consists of one inhomogeneous boundary, one homogenous boundary, two boundaries that are insulated to mass transport, and a zero initial condition. This requires that the mass transport coefficient of Eq. (9) be set to zero: $\mu_R = 0$. The exact solution to this problem is provided in Table 3.2.6 of Ref. [54]. The numerical solution was evaluated using a time step size of 10 s. Again the L^2 normalized error (L^2) is used to compare the numerical solution to the exact solution. The transient error is depicted in Fig. 5 with the anticipated exponential decay that approaches an error (L^2) of less than 0.0012. These results indicate that the solution is being solved accurately and correctly verifying the numerical model.

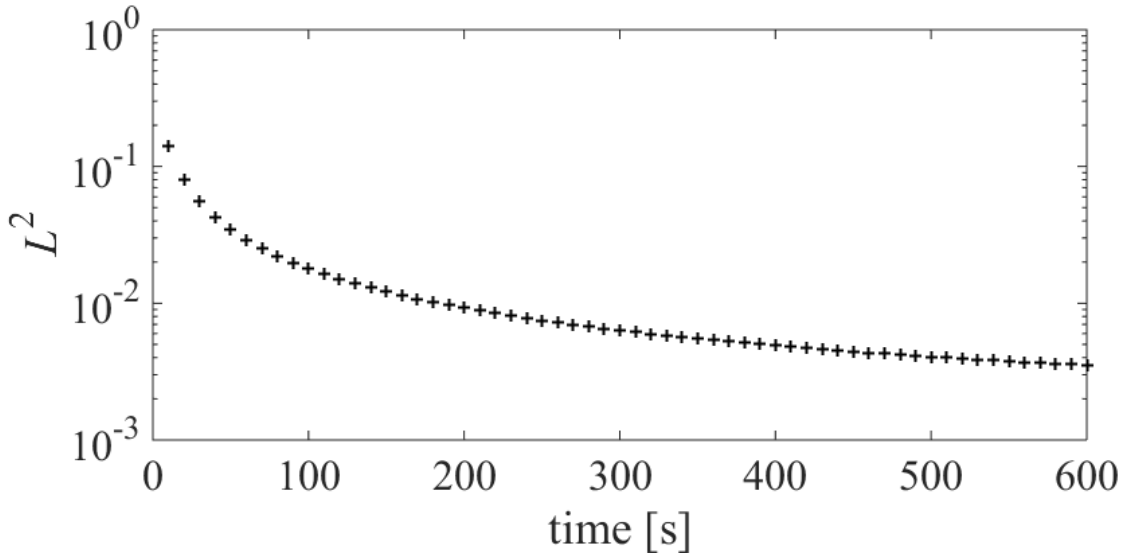

Fig. 5. The transient behavior of the normalized error (L^2) of Eq. (9) (where $\mu_R = 0$) compared to the corresponding exact solution presented in Table 3.26 of Ref. [54]

3.2. NUMERICAL HANDLING OF THE CONSERVATION EQUATIONS

Recall that Eq. (1) which governs the electric potential is nonlinear due to the dependence that the electrical conductivity has on the magnitude of the electric field (described by Eq. (3)). The computational handling of this nonlinearity is the focus of a number of studies [16, 21-23]. The most common method for determining the electric field distribution is the sequential analysis developed in Ref. [16]. However, in the comparison study of different methods in Ref. [23] it is shown that the nonlinear parametric analysis method (developed in Ref. [22]) provides a similar prediction of the electric field during tissue electroporation.

In this paper, the electric field is evaluated using the algorithm as shown in Fig. 6. The essence of this iterative approach is that the electrical conductivity is determined from the electrical field magnitude based on the potential distribution of the previous iteration. Note that this method allows the electrical conductivity to decrease during the iterative procedure, depending on the electric field magnitude. The final solution is achieved when the residual of the coupled electric potential and electrical conductivity Eqs. (1) and (3) is at a minimum. To help achieve convergence (solver stability), updating of the conductivity between iterations requires numerical damping:

$$\sigma^p\left(E,\sigma^{p-1}\right) = \omega\cdot\sigma(E) + \left(1-\omega\right)\cdot\sigma^{p-1} \tag{14}$$

where σ^p is the updated conductivity, σ^{p-1} is the conductivity from the last iteration, $\sigma(E)$ is evaluated using Eqs. (2) and (3), and ω is the numerical damping factor. The damping factor value used in this study is $\omega = 0.21$, providing the fastest rate of convergence.

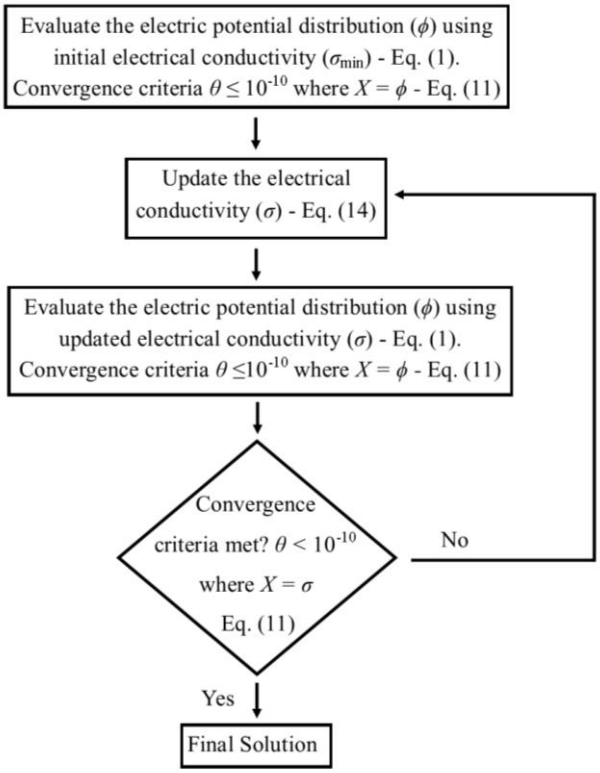

Fig. 6. The algorithm representing the iterative solving process used to determine the electric potential distribution and electrical conductivity for the electroporation pulse.

When solving for the first electroporation pulse (Fig. 6) the initial electrical conductivity is equal to the tissue in its normal state: no electroporation ($\sigma_{\text{int}} = \sigma_{\min}$). For the case of multiple electroporation pulses the initial electrical conductivity is determined using Eq. (7) ($\sigma_{\text{int}} = \sigma_R$). Note that when solving for the electric potential distribution (Fig. 6) the electrical conductivity should not be allowed to reduce below this initial value ($\sigma^p \geq \sigma_{\text{int}}$).

The conserved variables (C_e, C_i and ϕ), electrical conductivity (σ), and electric field magnitude (E) are evaluated at the cell centers. Due to the varying electrical conductivity (σ) the effective conductivity between cells is determined using a harmonic mean [55]. The electric field magnitude (E) of Eq. (2) is evaluated at the cell centers using an estimation of the electric potential (ϕ) at the cell interfaces using the conservation of flux. The degree of electroporation (DOE) and the fraction of irreversible electroporation (IE) are evaluated based on the electrical conductivity (σ). The conservation of intracellular (C_i) and extracellular concentration (C_e) are evaluated simultaneously using the transient mass transfer coefficient associated with the cellular uptake (μ_R - Eq. (11)) determined using the DOE_R evaluated at the current time step (t). Two types of boundary conditions (BC) are considered: Dirichlet BC (specified value) and zero flux Neumann BC (insulated).

3.3. CASE STUDIES

The two test cases considered in this study differ in electrode configuration: Case (1) is a parallel plate or side-by-side arrangement (Fig. 7a) and Case (2) is a clamped electrode arrangement (Fig. 7c). In both cases, the drug is introduced by a carrier gel that is applied to a single surface of the tissue as depicted in Fig. 7b and Fig. 7d.

The parameter values used in this study are provided in Table 1 and have been estimated to reflect the transport of calcien in liver tissue. Calcien was chosen for this study because its hydraulic radii and transport properties are well known [56]. The topical gel applied containing the calcien is assumed to have a diffusion coefficient of calcien in water at 37 °C.

The two cases are considered in a three stage process:

i. The pre-pulse diffusion stage: This consists of a one hour period during which drug is free to diffuse into the tissue from a topical applicator gel. Mass transport Eqs. (9) and (10) are evaluated numerically with $\mu_R = 0$.

ii. The electroporation pulse stage: Here the electroporation of a 100 μs duration pulse and its effects are modeled by solving Eqs. (1) - (5). At the conclusion of this stage the parameters DOE and IE have been established.

iii. The post-pulse diffusion stage: This consists of a ten minute long stage that accounts for the cellular uptake of the drug. Negligible cellular uptake occurs to living cells after ten minutes as resealing is approximately complete. During this stage the mass transport Eqs. (9) and (10) are evaluated numerically where the mass transport coefficient is numerically evaluated using Eqs. (6) and (11) at each time step.

Note that the electric pulse duration (stage ii) is specified as it is experimentally observed to influence the rate of cell permeability relaxation (τ) [48] and cell permeability to mass transport [38], but does not affect the evaluation of the steady state electric potential distribution (Eq. (1)).

The cases modeled both consist of a 2D domain composed of a simple homogenous section of liver tissue (Fig. 7). These cases described are for representative purposes and it should be noted that this model is not restricted to two dimensions, macroscopically homogenous tissue, or liver tissue specifically. The model uses a no-flux boundary condition on all the external surfaces of the domain in Fig. 7. For the electrical potential distribution this condition is justifiable if the boundaries are sufficiently far from the applied potential difference, not restraining the natural flow of electric current [13, 16]. Similarly, for drug transport, the boundaries are required to be sufficiently far from the drug source to have negligible influence on the drug diffusion. Thus, the domain used (Table 2) result in a good approximation of these conditions.

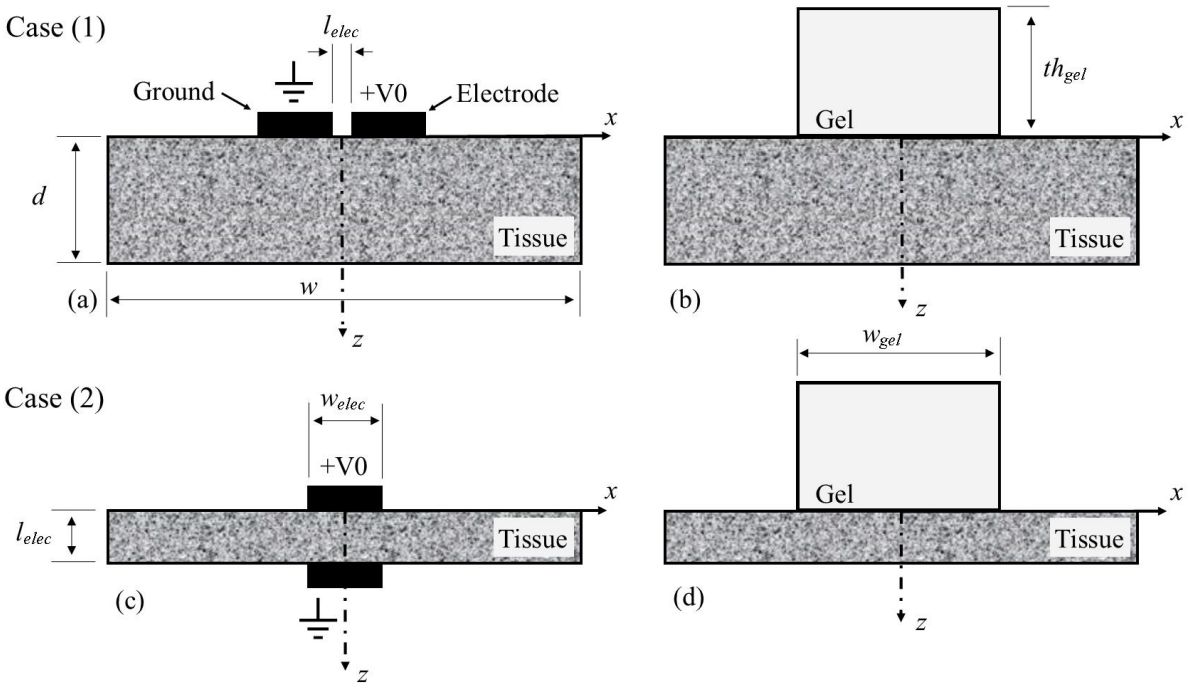

Fig. 7. Geometry of the two cases being modeled: Case (1) with both electrodes positioned on the surface and Case (2) with a clamped electrode configuration. (a) and (c) show the electric pulse setup and (b) and (d) show the drug gel applied to the top surface for Case (1) and (2) respectively.

3.4. MODEL PARAMETERS

The mass transfer coefficients related to cellular uptake ($\mu_{\max}$ and μ_0) are approximated for the purposes of this study using the theoretical electroporated cell representation developed by Miklavčič's research group in Ref. [43]. The resulting parameter values are provided in Table 1 for liver tissue consisting of hepatocyte cells which can be represented by a cube of equal side lengths [57].

For the case studies the diffusivity of calcien in the topical gel (D_{gel}) is approximated by the diffusivity of calcien in water at 37 °C (D_0) - determined theoretically using the Stokes-Einstein relation [56, 58]. The diffusivity of calcien in liver tissue (D_{eff}) is approximated theoretically using the free diffusivity of calcien in a dilute solution of water (D_0) and taking into account the tortuosity of the porous structure [51, 52]. However, this diffusivity (D_{eff}) neglects the interaction between the calcien and the extracellular structures [50]. The diffusivities determined provide an order of magnitude estimate, with a diffusivity of calcien in liver tissue comparable to that of the experimentally measured diffusion coefficient of calcien in brain tissue and a free diffusivity similar to the experimentally determined value for calcien in water [59, 60].

Table 1. Material Properties and Parameters (liver tissue)

Symbol	Description	Value	Reference
E_{rev}	Onset threshold for reversible electroporation	460 V/m	[16]
E_{irrev}	Onset threshold for irreversible electroporation	700 V/m	[16]
$\sigma_{\min}$	Tissue electrical conductivity with no electroporation	0.067 S/m	[16]
$\sigma_{\max}$	Maximum electrical conductivity due to electroporation	0.241 S/m	[16]
α	Sigmodal functional parameter	8	[16]
β	Sigmodal functional parameter	10	[16]
D_{gel}	Diffusivity calcien in gel (~calcien in water at 37 °C)	3.8×10^{-10} m^2/s	[56]
D_{eff}	Effective diffusivity of calcien in liver tissue	2.5×10^{-10} m^2/s	[52, 56]
ε	Volumetric porosity fraction	0.18	[61]
τ	Permeability decay time coefficient	100 s	[48]
μ_0	Minimum mass transfer coefficient of the cell membrane	0 1/s	[43]
$\mu_{\max}$	Maximum mass transfer coefficient of the cell membrane	9.4×10^{-5} 1/s	[1, 2, 26, 38, 43, 62]

Table 2. Model Parameters and Setup

Symbol	Description	Case (1)	Case (2)
V0	Applied voltage	480 V	350 V
C_{gel}	Initial drug concentration in the gel	1 kg/m^3	1 kg/m^3
d	Tissue thickness	10 mm	5 mm
w	Domain width	100 mm	100 mm
l_{elec}	Distance between electrodes	5 mm	5 mm
w_{elec}	Width of electrodes	20 mm	20 mm
th_{gel}	Gel thickness	10 mm	10 mm
w_{gel}	Gel width	50 mm	50 mm
t_{pre}	Pre-pulse diffusion duration	3600 s (1 hour)	3600 s (1 hour)
t_{post}	Post initial pulse diffusion duration	600 s (10 minutes)	600 s (10 minutes)
NOP	Number of spatial domain nodes	47306	110888
dt_{pre}	Time step size for the pre-pulse diffusion	10 s	10 s
dt_{post}	Time step size for the post-pulse diffusion	0.1 s	0.1 s

3.4. NONDIMENSIONALISATION

To study the mass transport in the system, the drug concentrations were nondimensionalized using the initial applied drug concentration (C_{gel}):

$$C_e^* = \frac{C_e}{C_{gel}} \tag{15}$$

$$C_i^* = \frac{C_i}{C_{gel}} \tag{16}$$

4. Results and Discussion

4.1. Pre-Pulse Drug Diffusion

Allowing the drug to diffuse into the tissue prior to the electroporation pulse, for a duration of an hour, results in an increase in extracellular drug concentration (C_e^*). The pre-pulse diffusion period (stage i) is critical as it allows the drug to diffuse into the tissue so that the extracellular drug concentration (C_e^*) is high in the region of tissue where it is later electroporated (stage ii). Figure 8 shows the extracellular concentration (C_e^*) contours from pre-pulse drug diffusion for both Case (1) and (2) (Fig. 7). Note that a significant amount of drug diffuses into the extracellular space at the top of the tissue.

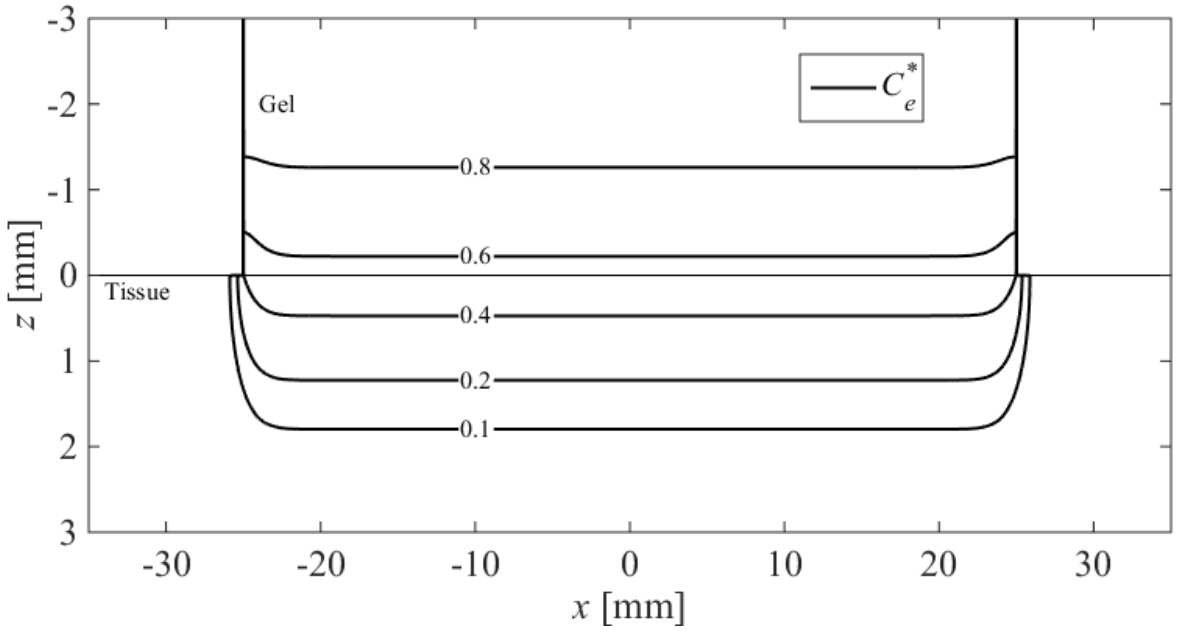

Fig. 8. Pre-pulse extracellular drug concentration (C_e^*) after leaving the drug to diffuse into the tissue for a duration of an hour for both Case (1) and (2).

4.2. Electroporation Pulse

An electrical pulse applied to the tissue, directly after the pre-pulse diffusion process, results in electroporation. Figure 9 shows the electric field magnitude (E) and the degree of electroporation (DOE). Figure 10 shows the fraction of irreversible electroporation (IE). For Case (1), a comparison of Fig. 9b and Fig. 10a shows a large portion of highly electroporated tissue is irreversibly electroporated and therefore dead. Case (1) produces a non-uniform distribution in electric potential resulting in a varying electric field magnitude (E) and thus large changes in the DOE (Fig. 9a and Fig. 9b). Whereas Case (2) results in a more uniform distribution in electric potential producing a region of highly and reversibly electroporated tissue ($DOE > 0.9$) - Fig. 9d. It is observed in Fig. 9 that

electroporation only occurs between the electrodes for both cases. This results in a smaller electroporated region for Case (1) (Fig. 9b).

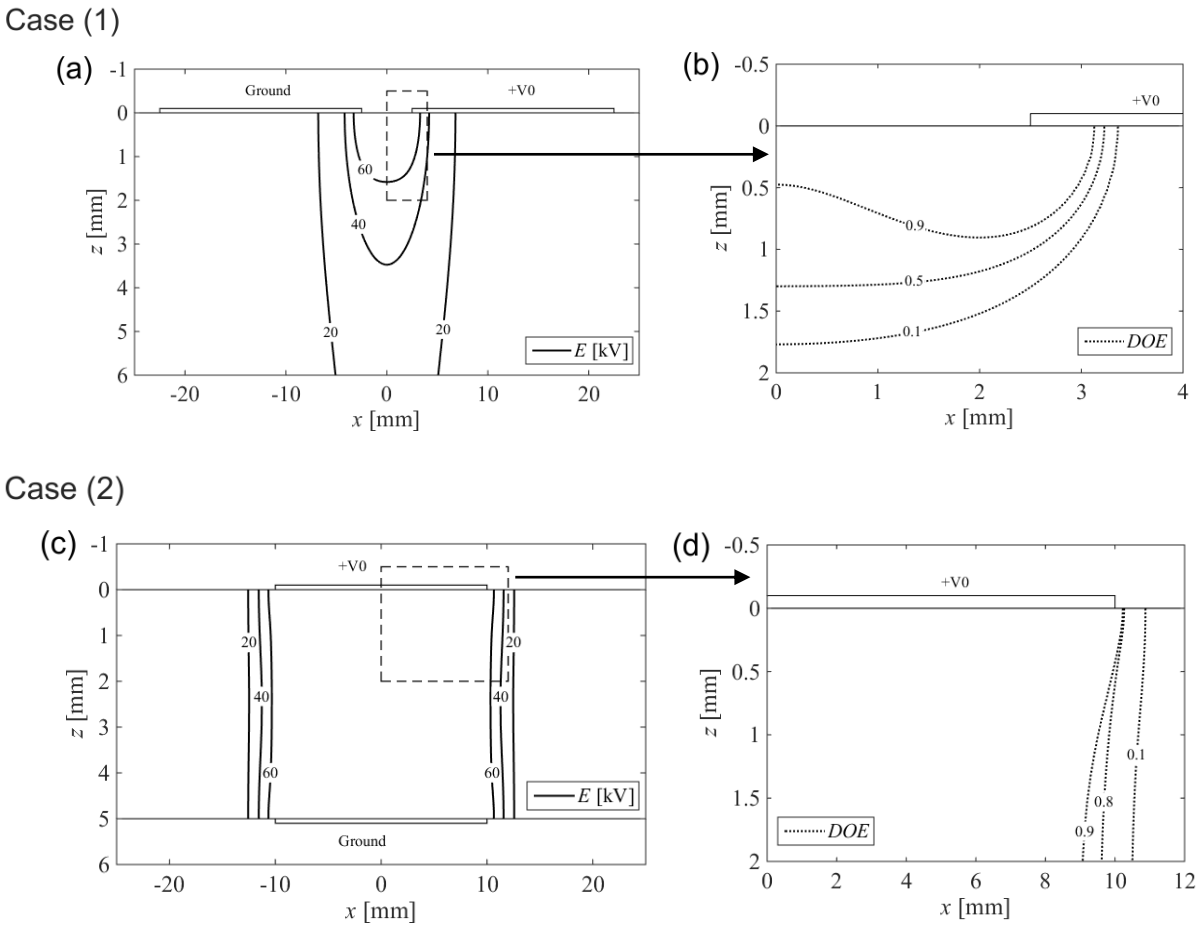

Fig. 9. An electric potential is applied between the electrode (+V0) and the ground for a duration of 100 μs resulting in electroporation of the liver tissue. (a) and (c) show the magnitude of electric field (E) [kV] and (b) and (d) show the subsequent degree of electroporation (DOE). The dashed boxes correspond to the sections depicted in (b) and (d) as well as in Fig. 10 and Fig. 12. Symmetry occurs about the z axis at $x = 0$ for both Case (1) and (2) and about the x axis at $x = 2.5$ [mm] for Case (2).

4.3. Post-Pulse Drug Diffusion

Drug transport in the tissue is considered for ten minutes after the electroporation pulse. Negligible cellular uptake occurs after ten minutes into reversibly electroporated cells due to cell resealing. Recalling that the main purpose of the electroporation is to increase the cellular drug uptake, Fig. 10 shows the intracellular concentration (C_i^*) and the fraction of irreversible electroporation (IE). The concentration gradient between extracellular and intracellular space due to the pre-pulse drug diffusion combined with increased cellular permeability (μ_R) allows significant cellular uptake to occur. The pre-pulse drug diffusion is therefore critical in the transmission of the drug to the cells as resealing occurs

relatively quickly. Unfortunately, in Case (1) (Fig. 10a) a large portion of the region where cellular drug uptake occurs has been irreversibly electroporated (*IE*). Case (2) provides a more optimal electrode setup for cellular drug uptake to living cells, where cellular uptake occurs in a larger region of tissue with a smaller fraction of this region being irreversibly electroporated (Fig. 10b).

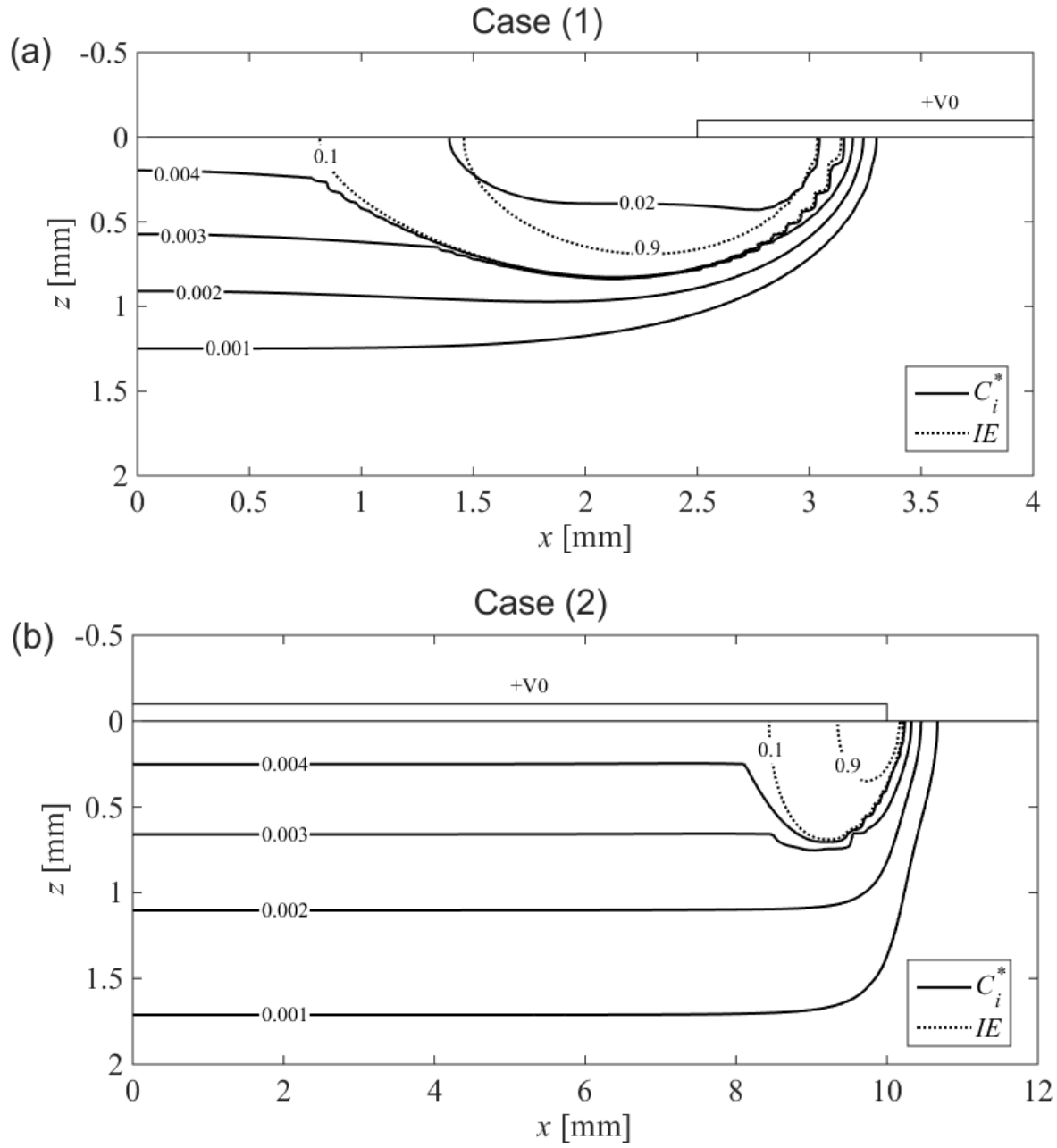

Fig. 10. After the single electroporation pulse the drug transport is considered for another 10 minutes with the applied drug gel removed. The increased rate of cellular uptake due to electroporation results in an increased intracellular drug concentration (C_i^*). Above the onset threshold of irreversible electroporation, the electric pulse results in a fraction of irreversible electroporation (*IE*).

The numerical values of cellular drug uptake are significantly larger in regions where irreversible electroporation occurs. This is because cell resealing significantly hinders the cellular uptake to living

cells. The application of multiple pulses spaced at intervals (periodic electroporation) would reduce the influence of pore resealing allowing cellular uptake to continue to occur.

4.4. PERIODIC ELECTROPORATION

Consider momentarily that the reversible portion of the transient degree of electroporation in Eq. (6), which is used to determine the cellular permeability in Eq. (11), has a time dependent exponential decay term. Equation (6) is rewritten here for clarity:

$$DOE_R(E,t) = DOE(E)\cdot\left(\left(1-IE(E)\right)\cdot \underbrace{\exp\left[-\frac{t_p}{\tau}\right]}_{resealing\ component} + IE(E)\right) \tag{17}$$

where the exponential decay in cellular permeability associated with pore resealing is labeled as the *resealing component*, and t_p corresponds to the time elapsed since the end of the previous pulse.

In this section we consider that the negative effect of pore resealing on delivery to cells can be moderated by implementing an electroporation pulse train so that the pores do not have the ability to fully reseal. Figure 11 illustrates the behavior of the *resealing component* (Eq. (17)) for a single pulse and for a train of pulses with a pulse spacing of 10 seconds, considered for a duration of 10 minutes.

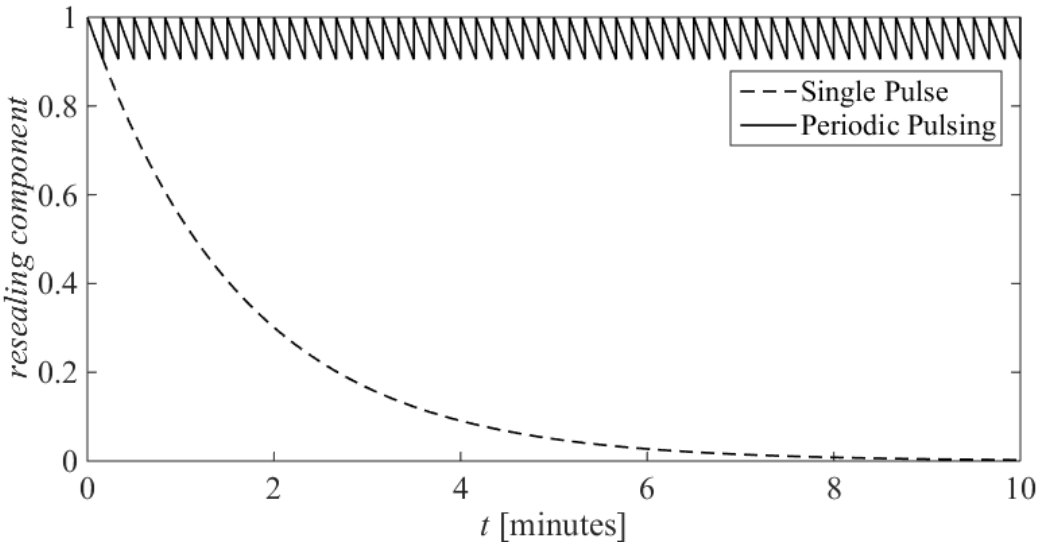

Fig. 11. The transient behavior of the *resealing component* of the transient degree of electroporation (Eq. (18)) for a single application of electroporation and for a pulse train where the tissue is electroporated periodically. The pulse train considered is applied for the entire 10 minutes with a pulse spacing of 10 seconds.

It is clear that the pulse train reduces the influence of pore resealing on the state of cellular permeability. With this in mind, we now present a study of Case (1) and (2) in which instead of a single pulse, pulses are administered at 10 second intervals over 10 minutes. After 10 minutes the final intracellular drug concentration (C_i^*) was evaluated and presented in Fig. 12 for both cases. The comparison of Fig. 12 to the previous cases using a single application of electroporation (Fig. 10) highlights the large increase, approximately fivefold, in intracellular drug concentration (C_i^*) in the reversible region ($IE < 0.1$) due to effectively removing the transient decay in cellular permeability (Fig. 11).

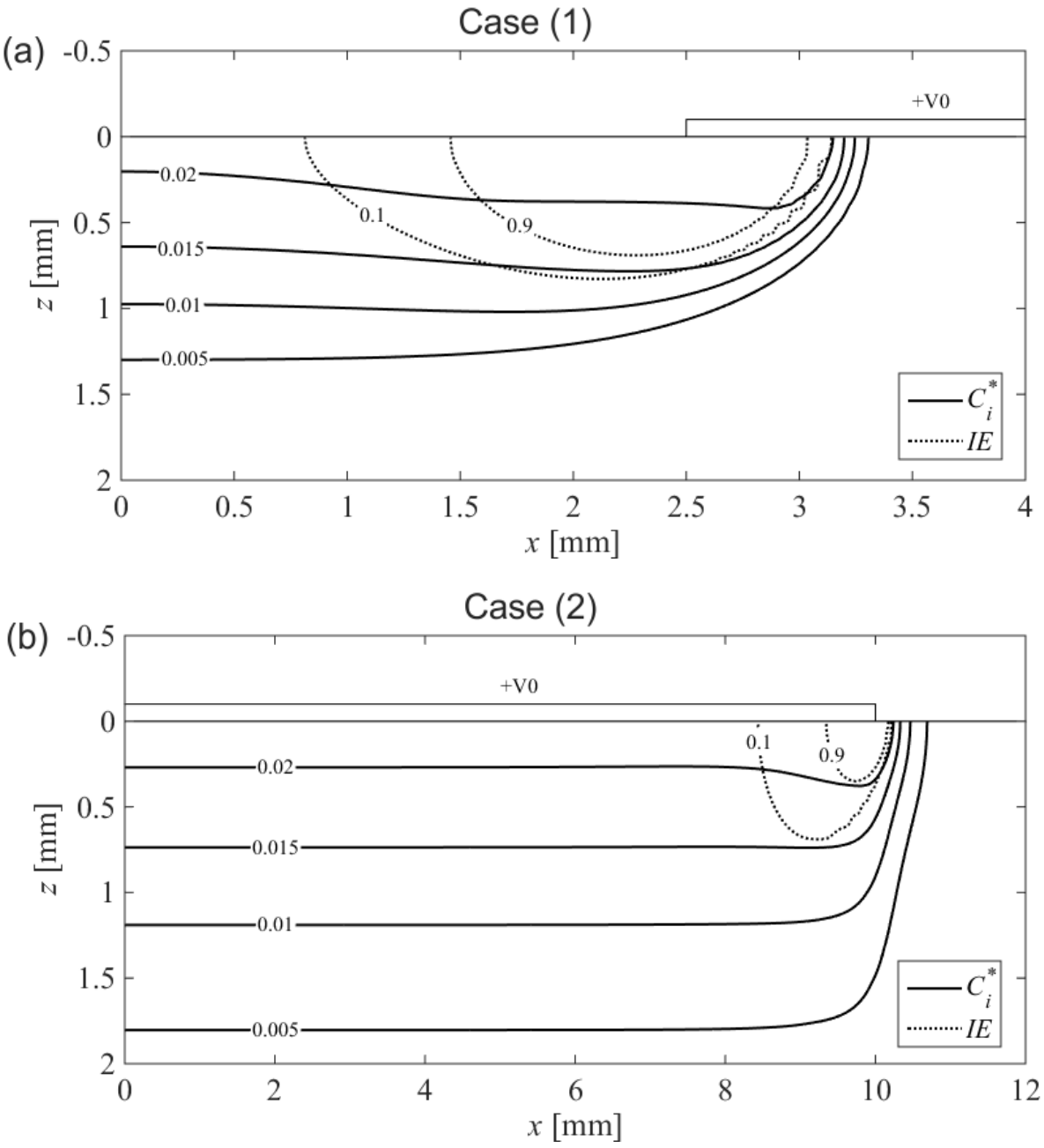

Fig. 12. After the first electroporation pulse of the pulse train the drug transport is considered for another 10 minutes with the applied drug gel removed. A pulse train with a pulse spacing of 10 seconds was applied for the entire 10 minutes in which drug transport was considered. The resulting intracellular drug concentration (C_i^*) and fraction of irreversible electroporation (IE) are depicted.

4.5. OPTIMIZATION

It is very apparent from the previous results that cellular drug uptake to living cells is limited by irreversible electroporation as it causes cell death. A study is conducted to determine the optimal pulse voltage when considering drug uptake to living cells, using the previously described cases where electroporation is applied periodically. In order to quantify the drug transported to living cells the dimensionless total drug mass in viable cellular space (m_i^*) is approximated by evaluating the integral of the intracellular drug concentration (C_i^*) over the domain for the portion of the tissue that is not irreversibly electroporated ($(1-IE)$ - viable portion):

$$m_i^*(t) = (1-\varepsilon) \int_{x=-w/2}^{w/2} \int_{z=0}^{d} \left(C_i^* \cdot (1-IE) \right) dxdz \tag{19}$$

where the porosity term $(1-\varepsilon)$ accounts for the use of the intrinsic volume averaged concentration (C_i^*) [51]. It is noteworthy to point out that Eq. (19) only considers the component of the mass that has been delivered to the viable living cells.

Equation (19) enables the total mass in viable cells (m_i^*) to be approximated for a specific case, allowing cases to be quantitatively compared and optimized. Following this logic a parametric study is considered; simulating the case studies using different applied voltages, in order to determine the optimal applied voltage when considering the maximization of m_i^* (Eq. (19)). Subsequently, the results for Case (1) and (2), using the periodic application of electroporation, are presented in Fig. 13, where the optimal voltage corresponds to the peak in the total drug mass in living cells (m_i^*). Clearly there seems to be an optimal voltage for each case (Case (1) ~ 480 V and Case (2) ~ 350 V). This is because as the magnitude of the applied electric field is increased, more cells are electroporated which results in more mass delivered to the viable cells. However, as the magnitude of the applied electric field is further increased, the portion of cells that is irreversibly electroporated increases.

The maximum total drug mass in living cells (m_i^*) for Case (2) is approximately five times larger than Case (1) due to the significantly larger region of electroporation and cellular uptake with a smaller fraction of this region being irreversibly electroporated (Fig. 10). Case (2) gives an optimal voltage when the extent of tissue electroporation is high, but still within the limits of reversibility ($DOE \approx 0.9$, near the onset of irreversible electroporation, E_{irrev}) - shown in Fig. 10b. Thus, the optimal voltage peak is also considered to be closely related to the maximization of reversible electroporation ($E \approx E_{irrev}$).

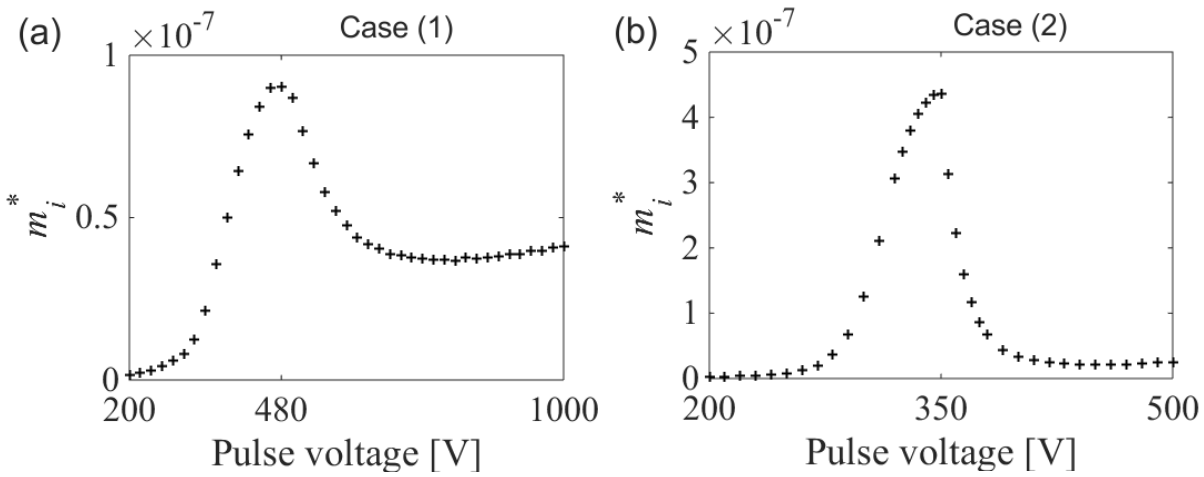

Fig. 13. The computed total mass in living cellular space (m_i^*) at different applied voltages using periodically applied electroporation every 10 seconds for a duration of 10 minutes (pulse train). The voltages resulting in the maximum cellular uptake to living cells for both cases (Case (1) ~ 480 V and Case (2) ~ 350 V) are used for the previously modeled results (Table 2).

5. CONCLUSION

This paper develops a macroscopic model of drug transport into biological tissue which is electroporated in order to increase cellular drug uptake. The model considers that the electrical conductivity of the tissue (which is easily measured) is a good indicator of the presence and state of the electropores at the cellular level. The model is based on the hypothesis that the DOE_R, which is based on the behavior of the tissue electrical conductivity, can be used to represent the state of cellular permeability to drugs.

While the model is primarily based on empirical observations, some of the relationships have not been fully established experimentally. The fraction of irreversibly electroporated cells in our model is evaluated from the electrical behavior of the tissue. The result approximates what is observed experimentally [11], however, further work is required to validate the accuracy of the relation. Furthermore, while the limits of the mass transfer coefficient (μ_R) are approximated theoretically in this study using experimentally determined properties, more work needs to be done to determine whether the rate of recovery of molecular permeability is equal to that of ionic permeability. Currently the model is limited to the use of empirical relationships from experimental results produced using specific conditions.

The development of this model did explicitly show that the electrode configuration plays a critical role in the success of the cellular uptake of the drug. It is also shown that a periodic electroporation regime can be implemented in order to offset the effects of pore resealing and that in our study, this results in five times the drug delivery (compared to a single pulse). It is also shown that the clamped electrode

configuration provides a larger region of reversible electroporation compared to the side-by-side arrangement.

6. Acknowledgment

The New Zealand Royal Society's Marsden Fund made the research possible.

7. References

1. Alberts, B., *Essential cell biology*. 2004, New York, NY: Garland Science.
2. Krassowska, W. and P.D. Filev, *Modeling Electroporation in a Single Cell.* Biophysical journal, 2007. **92**(2): p. 404-417.
3. Teissie, J., M. Golzio, and M.P. Rols, *Mechanisms of cell membrane electropermeabilization: A minireview of our present (lack of ?) knowledge.* BBA - General Subjects, 2005. **1724**(3): p. 270-280.
4. Weaver, J.C. and Y.A. Chizmadzhev, *Theory of electroporation: A review.* Bioelectrochemistry and Bioenergetics, 1996. **41**(2): p. 135-160.
5. Weaver, J.C., *Electroporation of biological membranes from multicellular to nano scales.* IEEE Transactions on Dielectrics and Electrical Insulation, 2003. **10**(5): p. 754-768.
6. Pavlin, M., V. Leben, and D. Miklavčič, *Electroporation in dense cell suspension—Theoretical and experimental analysis of ion diffusion and cell permeabilization.* Biochimica et Biophysica Acta (BBA) - General Subjects, 2007. **1770**(1): p. 12-23.
7. Pavlin, M. and D. Miklavčič, *Theoretical and experimental analysis of conductivity, ion diffusion and molecular transport during cell electroporation — Relation between short-lived and long-lived pores.* Bioelectrochemistry, 2008. **74**(1): p. 38-46.
8. Delemotte, L. and M. Tarek, *Molecular Dynamics Simulations of Lipid Membrane Electroporation.* The Journal of membrane biology, 2012. **245**(9): p. 531-543.
9. Tarek, M., *Membrane Electroporation: A Molecular Dynamics Simulation.* Biophysical Journal, 2005. **88**(6): p. 4045-4053.
10. Tieleman, D.P., *The molecular basis of electroporation.* BMC biochemistry, 2004. **5**(1): p. 10-10.
11. Puc, M., et al., *Quantitative model of small molecules uptake after in vitro cell electropermeabilization.* Bioelectrochemistry, 2003. **60**(1–2): p. 1-10.
12. Pavselj, N., et al., *The course of tissue permeabilization studied on a mathematical model of a subcutaneous tumor in small animals.* IEEE Transactions on Biomedical Engineering, 2005. **52**(8): p. 1373-1381.
13. Rubinsky, B., *Irreversible Electroporation*. 2009, Dordrecht: Springer Berlin Heidelberg.
14. Golberg, A. and M.L. Yarmush, *Nonthermal Irreversible Electroporation: Fundamentals, Applications, and Challenges.* IEEE Transactions on Biomedical Engineering, 2013. **60**(3): p. 707-714.
15. Rols, M.P. and J. Teissié, *Electropermeabilization of mammalian cells. Quantitative analysis of the phenomenon.* Biophysical journal, 1990. **58**(5): p. 1089-1098.
16. Sel, D., et al., *Sequential finite element model of tissue electropermeabilization.* Ieee Transactions on Biomedical Engineering, 2005. **52**(5): p. 816-827.
17. Davalos, R.V., B. Rubinsky, and D.M. Otten, *A feasibility study for electrical impedance tomography as a means to monitor tissue electroporation for molecular medicine.* IEEE Transactions on Biomedical Engineering, 2002. **49**(4): p. 400-403.
18. Pavlin, M. and D. Miklavčič, *Effective Conductivity of a Suspension of Permeabilized Cells: A Theoretical Analysis.* Biophysical journal, 2003. **85**(2): p. 719-729.
19. Pavlin, M., et al., *Effect of Cell Electroporation on the Conductivity of a Cell Suspension.* Biophysical journal, 2005. **88**(6): p. 4378-4390.
20. Čorović, S., L.M. Mir, and D. Miklavčič, *In Vivo Muscle Electroporation Threshold Determination: Realistic Numerical Models and In Vivo Experiments.* The Journal of membrane biology, 2012. **245**(9): p. 509-520.
21. Pavšelj, N., V. Préat, and D. Miklavčič, *A Numerical Model of Skin Electropermeabilization Based on In Vivo Experiments.* Annals of Biomedical Engineering, 2007. **35**(12): p. 2138-2144.

22. Lacković, I., R. Magjarević, and D. Miklavčič, *Incorporating Electroporation-related Conductivity Changes into Models for the Calculation of the Electric Field Distribution in Tissue*. 2010, Springer Berlin Heidelberg: Berlin, Heidelberg. p. 695-698.
23. Corovic, S., et al., *Modeling of electric field distribution in tissues during electroporation.* BioMedical Engineering Online, 2013. **12**(1): p. 16-16.
24. Granot, Y. and B. Rubinsky, *Mass transfer model for drug delivery in tissue cells with reversible electroporation.* International Journal of Heat and Mass Transfer, 2008. **51**(23): p. 5610-5616.
25. Mahnic-Kalamiza, S., D. Miklavcic, and E. Vorobiev, *Dual-porosity model of solute diffusion in biological tissue modified by electroporation.* Biochimica Et Biophysica Acta-Biomembranes, 2014. **1838**(7): p. 1950-1966.
26. Glaser, R.W., et al., *Reversible electrical breakdown of lipid bilayers: formation and evolution of pores.* Biochimica et biophysica acta, 1988. **940**(2): p. 275.
27. Klenchin, V.A., et al., *Electrically induced DNA uptake by cells is a fast process involving DNA electrophoresis.* Biophysical journal, 1991. **60**(4): p. 804-811.
28. Weaver, J.C., *Electroporation: A general phenomenon for manipulating cells and tissues.* Journal of cellular biochemistry, 1993. **51**(4): p. 426-435.
29. Tekle, E., R.D. Astumian, and P.B. Chock, *Selective and Asymmetric Molecular Transport Across Electroporated Cell Membranes.* Proceedings of the National Academy of Sciences of the United States of America, 1994. **91**(24): p. 11512-11516.
30. Rols, M.-P. and J. Teissié, *Electropermeabilization of Mammalian Cells to Macromolecules: Control by Pulse Duration.* Biophysical journal, 1998. **75**(3): p. 1415-1423.
31. Neumann, E., S. Kakorin, and K. Tœnsing, *Fundamentals of electroporative delivery of drugs and genes*. 1999, Elsevier S.A: LAUSANNE. p. 3-16.
32. Kotnik, T., et al., *Cell membrane electropermeabilization by symmetrical bipolar rectangular pulses: Part I. Increased efficiency of permeabilization.* Bioelectrochemistry, 2001. **54**(1): p. 83-90.
33. Tien, H.T. and A. Ottova, *The bilayer lipid membrane (BLM) under electrical fields.* IEEE Transactions on Dielectrics and Electrical Insulation, 2003. **10**(5): p. 717-727.
34. Davalos, R.V., L.M. Mir, and B. Rubinsky, *Tissue Ablation with Irreversible Electroporation.* Annals of Biomedical Engineering, 2005. **33**(2): p. 223-231.
35. Chen, C., et al., *Membrane electroporation theories: a review.* Medical & biological engineering & computing, 2006. **44**(1): p. 5-14.
36. Lee, R.C., *Cell Injury by Electric Forces.* Annals of the New York Academy of Sciences, 2006. **1066**(1): p. 85-91.
37. Esser, A.T., et al., *Towards solid tumor treatment by irreversible electroporation: Intrinsic redistribution of fields and currents in tissue.* Technology in Cancer Research and Treatment, 2007. **6**(4): p. 261-273.
38. Pavlin, M. and D. Miklavcic, *Theoretical and experimental analysis of conductivity, ion diffusion and molecular transport during cell electroporation - Relation between short-lived and long-lived pores.* BIOELECTROCHEMISTRY, 2008. **74**(1): p. 38-46.
39. Ivorra, A., et al., *In vivo electrical conductivity measurements during and after tumor electroporation: conductivity changes reflect the treatment outcome.* Physics in Medicine and Biology, 2009. **54**(19): p. 5949-5963.
40. Neal Ii, R.E. and R.V. Davalos, *The feasibility of irreversible electroporation for the treatment of breast cancer and other heterogeneous systems.* Annals of Biomedical Engineering, 2009. **37**(12): p. 2615-2625.
41. Lee, E.W., et al., *Electron microscopic demonstration and evaluation of irreversible electroporation-induced nanopores on hepatocyte membranes.* Journal of Vascular and Interventional Radiology, 2012. **23**(1): p. 107-113.
42. Saulis, G. and R. Saule, *Size of the pores created by an electric pulse: Microsecond vs millisecond pulses.* Biochimica et Biophysica Acta - Biomembranes, 2012. **1818**(12): p. 3032-3039.
43. Mahnič-Kalamiza, S., D. Miklavčič, and E. Vorobiev, *Dual-porosity model of solute diffusion in biological tissue modified by electroporation.* Biochimica et Biophysica Acta (BBA) - Biomembranes, 2014. **1838**(7): p. 1950-1966.
44. Meir, A. and B. Rubinsky, *Electrical impedance tomographic imaging of a single cell electroporation.* Biomedical Microdevices, 2014. **16**(3): p. 427-437.
45. Neal, R.E., et al., *In Vivo Irreversible Electroporation Kidney Ablation: Experimentally Correlated Numerical Models.* IEEE Transactions on Biomedical Engineering, 2015. **62**(2): p. 561-569.
46. Miklavčič, D., et al., *A validated model of in vivo electric field distribution in tissues for electrochemotherapy and for DNA electrotransfer for gene therapy.* BBA - General Subjects, 2000. **1523**(1): p. 73-83.

47. Puc, M., et al., *Quantitative model of small molecules uptake after in vitro cell electropermeabilization.* Bioelectrochemistry, 2003. **60**(1): p. 1-10.
48. Djuzenova, C.S., et al., *Effect of medium conductivity and composition on the uptake of propidium iodide into electropermeabilized myeloma cells.* BBA - Biomembranes, 1996. **1284**(2): p. 143-152.
49. Neumann, E., S. Kakorin, and K. Toensing, *Fundamentals of electroporative delivery of drugs and genes.* Bioelectrochemistry and Bioenergetics, 1999. **48**(1): p. 3-16.
50. Swartz, M.A. and M.E. Fleury, *Interstitial flow and its effects in soft tissues.* Annual Review of Biomedical Engineering, 2007. **9**(1): p. 229-256.
51. Becker, S. and A.V. Kuznetsov, *Transport in biological media*. 2013, Amsterdam; Boston: Elsevier/Academic Press.
52. Hrabe, J., S. Hrabětová, and K. Segeth, *A Model of Effective Diffusion and Tortuosity in the Extracellular Space of the Brain.* Biophysical journal, 2004. **87**(3): p. 1606-1617.
53. Young, D.M., *Iterative solution of large linear systems*. 1971, New York: Academic Press.
54. Myers, G.E., *Analytical methods in conduction heat transfer*. 1971, N.Y: McGraw-Hill.
55. Patankar, S.V., *Numerical heat transfer and fluid flow*. 1980, New York; Washington: Hemisphere Pub. Corp.
56. Prausnitz, M.R., et al., *Transdermal transport efficiency during skin electroporation and iontophoresis.* Journal of Controlled Release, 1996. **38**(2): p. 205-217.
57. Lodish, H.F., *Molecular cell biology*. 2008, New York: W.H. Freeman.
58. Cussler, E.L., *Diffusion: mass transfer in fluid systems*. 2009, New York; Cambridge: Cambridge University Press.
59. Magzoub, M., et al., *Extracellular Space Volume Measured by Two-Color Pulsed Dye Infusion with Microfiberoptic Fluorescence Photodetection.* Biophysical Journal, 2009. **96**(6): p. 2382-2390.
60. Becker, S., et al., *Transdermal transport pathway creation: Electroporation pulse order.* Mathematical biosciences, 2014. **257**: p. 60-68.
61. Goresky, C.A. and B.E. Nadeau, *Uptake of materials by the intact liver. The exchange of glucose across the cell membranes.* Journal of Clinical Investigation, 1974. **53**(2): p. 634-646.
62. Dechadilok, P. and W.M. Deen, *Hindrance factors for diffusion and convection in pores.* Industrial and Engineering Chemistry Research, 2006. **45**(21): p. 6953-6959.